Role of mode and intermediate waters in future ocean acidification: Analysis of CMIP5 models

L. Resplandy, L. Bopp, J. C. Orr, J. P. Dunne

Role of mode and intermediate waters in future ocean acidification: Analysis of CMIP5 models

L. Resplandy,[1] L. Bopp,[1] J. C. Orr,[1] and J. P. Dunne[2]

Received 31 January 2013; revised 21 March 2013; accepted 25 March 2013; published 18 June 2013.

[1] Consistent with recent observations, Coupled Model Intercomparison Project 5 Earth System Models project highest acidification rates in subsurface waters. Using seven Earth System Models, we find that high acidification rates in mode and intermediate waters (MIW) on centennial time scales (–0.0008 to –0.0023 ± 0.0001 yr^{-1} depending on the scenario) are predominantly explained by the geochemical effect of increasing atmospheric CO_2, whereas physical and biological climate change feedbacks explain less than 10% of the simulated changes. MIW are characterized by a larger surface area to volume ratio than deep and bottom waters leading to 5 to 10 times larger carbon uptake. In addition, MIW geochemical properties result in a sensitivity to increasing carbon concentration twice larger than surface waters ($\Delta[H^+]$ of $+1.2 \times 10^{-4}$ mmol m^{-3} for every mmol m^{-3} of dissolved carbon in MIW versus $+0.6 \times 10^{-4}$ in surface waters). Low pH transported by mode and intermediate waters is likely to influence surface pH in upwelling regions decades after their isolation from the atmosphere. **Citation:** Resplandy, L., L. Bopp, J. C. Orr, and J. P. Dunne (2013), Role of mode and intermediate waters in future ocean acidification: analysis of CMIP5 models, *Geophys. Res. Lett.*, *40*, 3091–3095, doi:10.1002/grl.50414.

1. Introduction

[2] Over the past decades, the ocean has been undergoing physical and biogeochemical modifications in response to human-induced global change [*Bindoff et al*., 2007], in particular a reduction of pH altering fundamental chemical balances commonly referred to as ocean acidification (refer to *Doney et al.* [2009] for a review). Since 1750, the ocean has absorbed about 30% of the total anthropogenic emission of CO_2 [*Sabine et al*., 2004], resulting in a decrease of the oceanic pH of 0.1 unit at the surface (Royal Society, [*Raven et al*., 2005]). This ocean acidification may impact marine organisms by rendering the environment for calcifying marine plankton less hospitable [*Hofmann et al.*, 2010] and by imposing greater physiological stress [*Pörtner*, 2008].

[3] Observed surface pH changes of ∼ –0.0017 to –0.0019 yr^{-1} in the North Atlantic and the North Pacific are consistent with that expected for seawater in equilibrium with the atmosphere [*Dore et al.*, 2009; *Byrne et al.*, 2010; *González-Dávila et al.*, 2010; *Bates et al.*, 2012]. Interestingly, in both basins, highest rates of acidification are observed at the subsurface [*Dore et al.*, 2009; *Byrne et al.*, 2010; *Bates*, 2012], where typical subtropical mode waters are located [*Hanawa and Talley*, 2001]. While observational studies suggest that this subsurface maximum in acidification rates results from changes in circulation and biological activity [*Dore et al.*, 2009; *Byrne et al.*, 2010], ocean carbon cycle models suggest that changes in the carbonate chemistry alone can explain the observed changes [*Orr*, 2011].

[4] Although the physical and chemical basis for ocean acidification is well understood, the processes explaining the presence of higher acidification rates at the subsurface are not well constrained, and the possible impacts at the global scale are unknown. Consistent with the observations, the latest version of Earth System Models (ESMs) future projections simulate highest acidification rates in subsurface in sub-tropical oceans. Here, we use these ESMs to evaluate subsurface acidification rates (section 3), constrain the driving mechanisms (section 4), and discuss the possible impacts on surface pH (section 5).

2. Methods

2.1. Description of Models and Simulations

[5] We use the latest generation of projections performed by seven Earth System Models in the frame of the Coupled Model Intercomparison Project 5 (CMIP5, *Taylor et al.* [2012]), all of which simulated 3-D pH field for at leat one of the four future climate change scenarios and for the control simulation (see Table 1). Scenarios RCP2.6, RCP4.5, RCP6.0, and RCP8.5 are representative concentration pathways (i.e., RCP) with additional radiative forcing of 2.6, 4.5, 6, and 8.5 $W.m^2$. CO_2 atmospheric concentrations reach 421, 538, 670, and 936 ppm in 2100 for each of these four scenarios. Results of these four scenarios are used to evaluate the sensitivity of the system to the strength of the forcing. Whereas atmospheric CO_2 concentration in RCP4.5, RCP6.0, and RCP8.5 increases from 2006 to 2100, the concentration in RCP2.6 declines after peaking in 2050. This "peak-and-decline" scenario was used to track changes after the decline of CO_2 emissions. In addition, a sensitivity simulation (called esmFdbk2), including the increased radiative forcing of scenario RCP4.5 but no increase in atmospheric CO_2 concentration, was used to isolate the contribution of climate change feedbacks (changes in ocean circulation, biological activity, etc.) from the chemical

All supporting information may be found in the online version of this article.

[1]Laboratory for Science of Climate and Environment, IPSL, CEA-UVSQ-CNRS, Paris, France.
[2]National Oceanic and Atmospheric Administration/Geophysical Fluid Dynamics Laboratory, Princeton, New Jersey, USA.

Corresponding author: L. Resplandy, Laboratory for Science of Climate and Environment, IPSL, CEA-UVSQ-CNRS, Gif-sur-Yvette, Paris, France. (laure.resplandy@lsce.ipsl.fr)

0094-8276/13/10.1002/grl.50414

Table 1. CMIP5 Models Used in This Study

Models	Avail. Scenarios (RCPs)	Ref.
CESM1-BGC	4.5, 8.5	*Gent et al.* [2011]
GFDL-ESM2G	2.6, 4.5, 6.0, 8.5	*Dunne et al.* [2012]
GFDL-ESM2M	2.6, 4.5, 6.0, 8.5, exmFdbk2	*Dunne et al.* [2012]
IPSL-CM5A-LR	2.6, 4.5, 6.0, 8.5, exmFdbk2	*Séférian et al.* [2012]
IPSL-CM5A-MR	2.6, 4.5, 8.5	*Séférian et al.* [2012]
MPI-ESM-MR	2.6, 4.5, 8.5	*Giorgetta et al.* [2013][a]
NorESM1-ME	2.6, 4.5, 6.0, 8.5	*Bentsen et al.* [2012]

[a] Giorgetta M. A., et al. [(2013)], The Community Climate System Model version 4, submitted to *Journal of Advances in Modeling Earth Systems*.

effect of increasing CO_2 concentration. The control simulation is used to correct the estimated trends from model drift. CMIP5 ESMs provide pH on the total scale. We take the model spread, namely the standard deviation, as an indicator of uncertainty for a given projection. Note that although the uncertainty depends on the number of models available for each scenario, it is relatively small compared to the considered changes. To facilitate inter-model comparison, all variables were interpolated onto a common $1° \times 1°$ regular grid using a Gaussian weighted average and to standard ocean depths (World Ocean Atlas levels) using linear interpolation.

2.2. Water Mass Framework

[6] The distribution of oceanic water masses differs in the various models leading to the comparison of dissimilar characteristics and large inter-model differences when using a point-by-point analysis. In this study, we used a global framework to group together water masses of similar behavior. Four classes were defined: Stratified Tropical Waters (STW), Mode and intermediate Waters (MIW), Deep Waters (DW), and Bottom Waters (BW). For example, the class MIW aims at gathering mode and intermediate waters of all basins, which share common features but are not distributed in the same density range [*Hanawa and Talley*, 2001]. Limits between these different water masses were defined using dynamical criteria (stratification, meridional velocities, etc.) sometimes resulting in different density thresholds for the five different basins: North Atlantic, South Atlantic, North Pacific, South Pacific, and Indian Ocean. Note that the Arctic is not included. These density thresholds were computed for each model using the first 10 years of the medium change RCP4.5 scenario (temperature, salinity, and meridional velocity) and the potential density referenced to 2000 m ($\sigma 2$).

[7] The limit between the well stratified STW and the homogeneous MIW was defined using a stratification criteria, with STW including all depths above $\frac{\partial \sigma 2}{\partial z} = 0.02$ kg m^{-4}. The lower boundary of MIW was defined as the depth below which the salinity reaches the value at the deep salinity minimum plus 0.05. Deep waters (DW) were distinguished from bottom waters (BW) using the deepest level where there is a change in sign of meridional velocities, orientated northward in BW and southward in DW. One exception is the North Atlantic MIW, which does not have a deep salinity minimum. Instead, the limit between MIW and DW was defined as the 8°C isotherm.

3. Acidification in Mode and Intermediate Waters

[8] The pH simulated along sections in the Pacific Ocean (190°E, Figure 1a) and the Atlantic Ocean (330°E, see Supporting Information) by the GFDL-ESM2M model is shown for the first decade of the RCP8.5 scenario (2006–2016). In agreement with in situ observations [*Byrne et al.*, 2010, Figure 1], surface pH exhibits a typical distribution with high surface values (∼8.1) decreasing slightly in the equatorial upwelling region. At depth, pH decreases due to CO_2 production from organic matter remineralization, with pH minimum values at 400–1000 m coinciding with oxygen minimum levels.

[9] The 80-year pH difference ($\Delta pH = \overline{pH}_{2086:2096} - \overline{pH}_{2006:2016}$) in the "business as usual" RCP8.5 scenario shows declining pH (Figure 1c). Major changes are located between the surface and ∼1000 m, in what is identified as Stratified Tropical waters (STW) and Mode and Intermediate

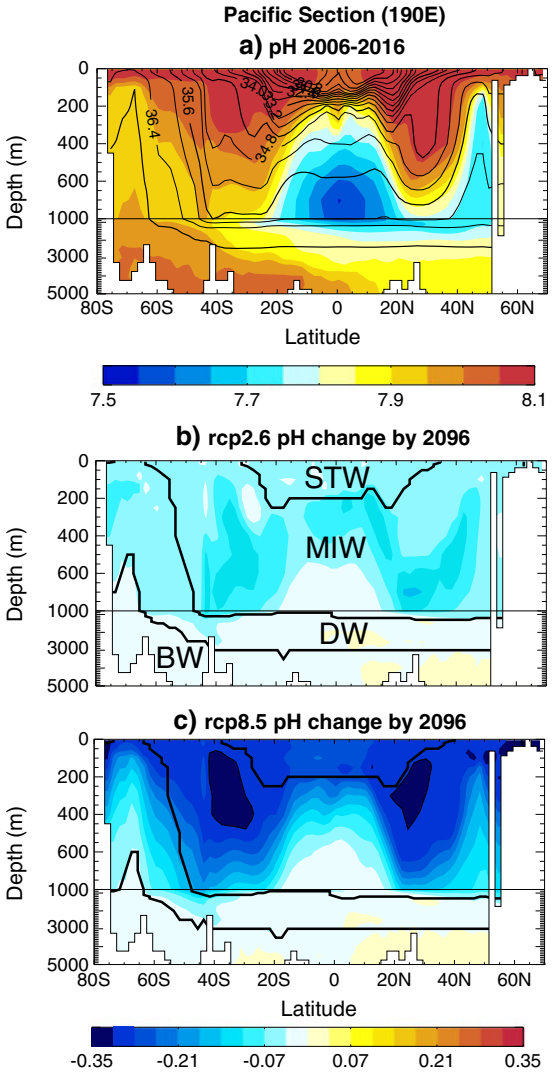

Figure 1. Pacific section at 190°E in GFDL-ESM2M. (a) pH averaged for 2006–2016 in RCP8.5 overlaid with $\sigma 2$. (b and c) Change in pH by 2096 in Figure 1b RCP2.6 and Figure 1c RCP8.5 overlaid with water masses contours (see section 2.2). The change in pH is computed as the difference between the 2086–2096 and 2006–2016 decades.

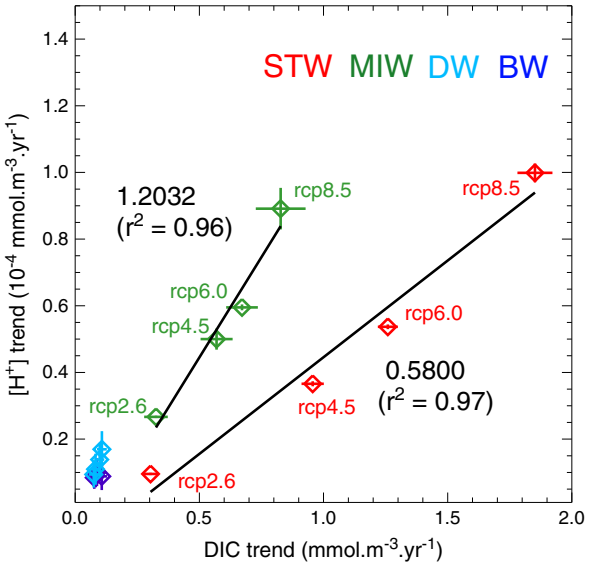

Figure 2. Model-mean global trends of total H^+ concentration versus DIC for RCP2.6, RCP4.5, RCP6.0, and RCP8.5 in Stratified Tropical Waters (STW), Mode and Intermediate Waters (MIW), Deep Waters (DW), and Bottom Waters (BW). Model spread is indicated by error bars (± 1 std). Trends were computed between 2006 and 2096. See section 2.2 for details on water mass definition.

Waters (MIW, see section 2.2 for details on method). pH changes are maximum in upper MIW (–0.35). In contrast, the acidification of Bottom (BW) and Deep (DW) waters is much weaker and mostly confined to the region of deep water formation in the Southern Ocean (Figures 1a and 1c). The pH response in the "peak-and-decline" RCP2.6 scenario shares common features with the response in RCP8.5: pH reduction is largest in MIW (–0.10) and smallest in DW and BW. The difference in amplitude between the response in RCP2.6 and RCP8.5 scenarios arises from the difference in the atmospheric CO_2 concentration, which is more than twice as high at the end of this century in RCP8.5 than in RCP2.6 (421 versus 936 ppm). Another difference is that ΔpH in RCP2.6 is particularly low in STW and upper MIW. Indeed, pH changes in those waters closely mirror the evolution of atmospheric CO_2, which increases continuously between 2006 and 2100 in RCP8.5, whereas it decreases after 2050 in the "peak-and-decline" RCP2.6 scenario.

[10] We extended this analysis to the seven ESMs, by considering the model-mean response averaged globally in the four water masses. The main results identified along the Pacific section in GFDL-ESM2M (Figure 1) hold true at the global scale and for all ESMs. Major pH reductions are observed in STW and MIW, with trends ranging from –0.0004 yr^{-1} (RCP2.6) to –0.0035 yr^{-1} (RCP8.5) in STW and from –0.0008 yr^{-1} (RCP2.6) to –0.0023 yr^{-1} (RCP8.5) in MIW and in all cases, there is close model agreement (standard deviation < 0.0001) (Figure 2). Although highest rates of acidification are located in upper MIW, when averaged over the water mass volume pH trends are larger in STW than in MIW. In agreement with results along the Pacific section, changes in DW and BW are weak with global trends < –0.0004 ± 0.0001 yr^{-1} in all scenarios (Figure 2).

4. Chemical Versus Climate Change Contribution to Acidification

[11] In the following, we examine the contributions of biological and physical changes associated with climate change and of chemical changes associated with increasing atmospheric CO_2 in the acidification of MIW. Climate change could increase the CO_2 uptake and hence the pH of one water mass by increasing its outcrop surface, i.e., the exchange surface between this water mass and the atmosphere [*Séférian et al.*, 2012] or by changes in transport and biological production of CO_2 (remineralization) in the ocean interior [*Byrne et al.*, 2010; *Bates*, 2012]. Although outcrop surfaces in the seven ESMs are modified by climate change, their changes cannot explain the higher acidification rates in MIW. Indeed, ESMs predict a decrease of MIW (–11.6 ± 2.6%), DW (–26.4±6.7%), and BW (–48.1±22.7%) outcrop surfaces compensated by an increase of the STW outcrop surface (+24.1 ± 5.5%).

[12] The contribution of climate change feedbacks (circulation, biological activity, etc.) is estimated using a sensitivity experiment based on the scenario RCP4.5 and available for two of the seven models (see details on experiment esmFdbk2 in section 2.1). pH trends in MIW in this sensitivity experiment (<0.0001 yr^{-1} in GFDL-ESM2M and IPSL-CM5A-LR) represent less than 10% of the total pH trend found with scenario RCP4.5 (–0.0014 yr^{-1} and –0.0016 yr^{-1}, respectively). This is explained by the relatively small effect that productivity, respiration, and circulation changes have on H^+ concentration when compared to the effect of increasing atmospheric CO_2 (280 to 538 ppm in RCP4.5). As previously shown for surface waters [*Orr et al.*, 2005], this suggests that on centennial time scales, the geochemical effect of increasing atmospheric CO_2 largely dominates the high acidification rate in MIW, while climate change feedbacks only play a minor role. This is also consistent with the results obtained with older versions of ocean carbon cycle models that did not account for climate change feedbacks and still projected a sub-subsurface maximum in acidification rates [*Orr*, 2011].

[13] From the synthesis of all RCP scenarios and available models, we find that the acidification rates in STW and MIW are linearly correlated to the increase in dissolved inorganic carbon (DIC) concentration in these water masses (Figure 2). As expected from the Revelle factor $\left(\frac{\partial pCO_2/pCO_2}{\partial DIC/DIC}\right)$ that increases from low latitudes to high latitudes [*Orr*, 2011], STW have higher DIC concentrations than does MIW (Figure 2). However, the sensitivity to increasing carbon concentration $\left(\text{noted } \frac{\partial[H^+]}{\partial DIC}\right)$ in MIW is 50% larger than in STW: for every mmol m^{-3} increase in DIC, $[H^+]$ increases by ∼ 0.6×10^{-4} mmol m^{-3} in STW and by ∼ 1.2×10^{-4} mmol m^{-3} in MIW (Figure 2). This

Table 2. Averaged Values in STW and MIW for the IPSL-CM5A-LR Model in 2006, i.e. at the Beginning of All RCP Scenarios

	STW 2006	MIW 2006
pH (total scale)	7.79	7.94
temperature (°C)	23.9	9.6
DIC (mmol m^{-3})	2105	2257
salinity (practical scale)	35.28	34.97
alkalinity (mmol m^{-3})	2435	2422

difference in the $\frac{\partial[H^+]}{\partial DIC}$ ratio can be attributed to the different geochemical properties of MIW and STW. The impact of temperature, salinity, alkalinity, and DIC concentration on $\frac{\partial[H+]}{\partial DIC}$ is examined using averaged values typical of STW and MIW in the IPSL-CM5A-LR model (Table 2) and the CO2calc program [*Molines et al.*, 2010]. The lower temperature and lower alkalinity in MIW (see Table 2) each result in increasing $\frac{\partial[H^+]}{\partial DIC}$ by ∼30% relative to its STW value. Furthermore, DIC concentrations are generally larger in MIW than in STW (see Table 2), increasing the MIW $\frac{\partial[H^+]}{\partial DIC}$ by an extra 30% relative to STW. In contrast, the difference in salinity between MIW and STW does not affect $\frac{\partial[H^+]}{\partial DIC}$. It is interesting to note that DW and BW are even more sensitive to increasing carbon concentration $\left(\frac{\partial[H^+]}{\partial DIC} = 2.2\text{in DW}\right)$ than MIW due to their lower temperature, lower alkalinity, and higher DIC concentration. However, DW and BW exhibit relative surface area to volume ratios (outcrop surface / water mass volume), respectively ∼15 and ∼30 times smaller than the one of MIW, resulting in DIC uptake 3 to 10 times smaller (Figure 2). What makes MIW particularly vulnerable to ocean acidification is the combination of 1) their high sensitivity to increasing CO_2, double that of STW, and 2) their large surface area for air-sea exchange relative to its volume, which is much larger than for DW and BW.

[14] Although changes in circulation and biological activity are relatively small on centennial time scales, they might play a larger role on interannual and decadal time scales. A ventilation slow-down and an increased biological production of CO_2 in the ocean interior during the 1990s were identified as the major drivers of high acidification rates observed at the subsurface in the North Pacific [*Deutsch et al.*, 2006; *Dore et al.*, 2009; *Byrne et al.*, 2010]. In addition, observations suggest that the decadal North Atlantic Oscillation modulates the CO_2 uptake and hence the pH in the North Atlantic mode waters [*Bates*, 2012]. At the subsurface, we find that the amplitude of pH trends attributed to increasing atmospheric CO_2 concentration at the centennial time scales (–0.0010 to –0.0040 yr^{-1}, in this study) are of the same order of magnitude as pH trends previously attributed to processes at the decadal time scales (up to –0.0020 unit yr^{-1}, *Byrne et al.*, [2010]). This contrasts with the recent study of *Friedrich et al.* [2012] pointing out that surface pH changes associated with external anthropogenic forcing largely exceeds those associated with natural variability at the regional scale. However, the fact that the surface area to volume ratio of MIW is one order of magnitude smaller than the one of STW highlights the stronger influence of atmospheric forcing on STW than on MIW. This explains the apparent discrepancy between the contribution of anthropogenic forcing relatively to the contribution of natural variability evaluated at the surface [*Friedrich et al.*, 2012] and at the subsurface (this study). The contribution of anthropogenic forcing in the acidification of subsurface waters increases over time in conjunction with the transport of mode and intermediate waters into the ocean interior and will probably largely exceed the natural variability in the future.

5. Implications for Surface pH

[15] The high sensitivity of MIW to increasing atmospheric CO_2 is likely to have an impact on acidification

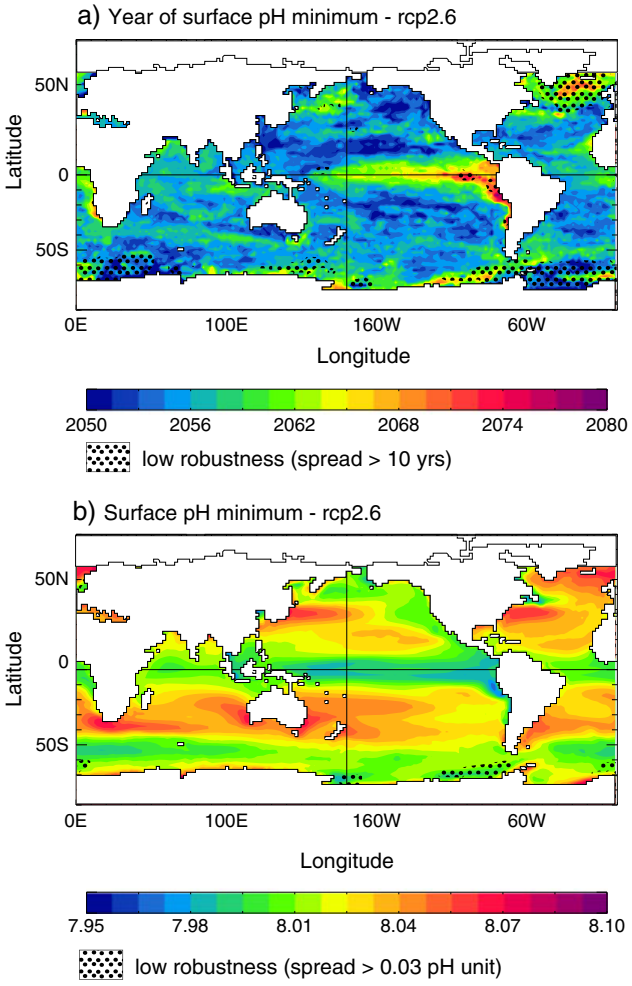

Figure 3. Model-mean pH in RCP2.6 scenario: (a) year of surface pH minimum, (b) surface pH minimum value. Stippling indicates poorer agreement, i.e., where the model spread is larger than: (Figure 3a) 10 years and (Figure 3b) 0.03 pH unit. Figure based on the six models with pH for RCP2.6 (GFDL-ESM2G, GFDL-ESM2M, IPSL-CM5A-LR, IPSL-CM5A-MR, MPI-ESM-MR, and NorESM1-ME).

at the global scale. This impact is assessed here using the "peak-and-decline" scenario (see details on RCP2.6 in section 2.1). In subtropical gyres, surface pH is at least 1 to 5 years after the peak in atmospheric CO_2 in 2050, confirming that in the regions where decadal time series are located (BATS, HOT, ESTOC), surface pH mirrors atmospheric CO_2 (Figure 3). However, in some regions, in particular in upwelling regions (Equatorial Pacific, Benguela, Peru-Chile, Arabian Sea, etc.) and deep convection regions (North Atlantic and Southern Ocean), the surface pH is minimum 10 to 30 years after atmospheric CO_2 decline has started (Figure 3). Indeed, low pH mode and intermediate waters formed at medium and high latitudes are subducted and isolated from the atmosphere, advected in the ocean interior towards lower latitudes where they are mixed with lighter waters (diapycnal mixing) and finally reach the surface in upwelling regions. The time scale of 10–30 years identified here is consistent with the upwelled waters being a mixture of STW, in which the pH minimum closely follows the 2050 peak in atmospheric CO_2, and MIW, which

typically require 30 to 100 years to transport the pH minimum from where they are formed to where they are upwelled to the surface [*Rodgers et al.*, 2003]. In contrast, the signature detected in the North Atlantic and the Southern Ocean, which is less robust across the seven models (Figure 3), can be attributed to spatial and temporal changes in deep convection favoring mixing with deep low pH waters in some of the models.

6. Conclusions

[16] We used seven CMIP5 ESMs to distinguish the intensity and controls of mode and intermediate water acidification. Using a water-mass framework, we showed that high anthropogenic acidification rates predicted in mode and intermediate waters on centennial time-scales stem from their chemical and physical properties. Mode and intermediate waters capture more carbon than deep and bottom waters because of their larger surface area that exchanges with the atmosphere relative to their volume. In addition, their acidification rate is twice more sensitive to increasing carbon concentration than the rate in stratified surface waters due to lower temperature, higher carbon concentration, and lower alkalinity. Moreover, the low pH of mode and intermediate waters will affect regions where they are upwelled decades later and far from their time and place of subduction.

[17] **Acknowledgments.** We sincerely thank R. Séférian for the useful discussions and two anonymous reviewers for their helpful comments on the manuscript. This work was made possible, thanks to the climate modeling groups (Table 1) for producing and making available their model output. We are grateful to P. Brockmann and the IPSL team for making the access to the CMIP5 database so easy. We acknowledge the World Climate Research Programme's Working Group on Coupled Modelling, which is responsible for CMIP. Support was provided by the EU FP7 project CARBOCHANGE, "Changes in carbon uptake and emissions by oceans in a changing climate", which received funding from the European Commissions Seventh Framework Programme under grant agreement 264879. For CMIP, the U.S. Department of Energy's Program for Climate Model Diagnosis and Intercomparison provides coordinating support and led development of software infrastructure in partnership with the Global Organization for Earth System Science Portals. The Editor thanks two anonymous reviewers for their assistance in evaluating this paper.

References

Bates, N. R. (2012), Multi-decadal uptake of carbon dioxide into subtropical mode water of the North Atlantic Ocean, *Biogeosciences*, *9*(7), 2649–2659, doi:10.5194/bg-9-2649-2012.

Bates, N. R., M. H. P. Best, K. Neely, R. Garley, A. G. Dickson, and R. J. Johnson (2012), Detecting anthropogenic carbon dioxide uptake and ocean acidification in the North Atlantic Ocean, *Biogeosciences*, *9*(7), 2509–2522, doi:10.5194/bg-9-2509-2012.

Bentsen, M., et al. (2012), The Norwegian Earth System Model, NorESM1-M Part 1: Description and basic evaluation, *Geosci. Model Dev. Discuss.*, *5*, 2843–2931.

Bindoff, N. L., et al. (2007), Observations: Oceanic climate change and sea level, in *Climate Change 2007: The Physical Science Basis. Contribution of Working Group I to the Fourth Assessment Report of the Intergovernmental Panel on Climate Change*, edited by S. Solomon, D. Qin, M. Manning, Z. Chen, M. Marquis, K. Averyt, M. Tignor, and H. Miller, 48 pp., Cambridge University Press, Cambridge, UK.

Byrne, R. H., S. Mecking, R. A. Feely, and X. Liu (2010), Direct observations of basin-wide acidification of the North Pacific Ocean, *Geophys. Res. Lett.*, *37*, L02601, doi:10.1029/2009GL040999.

Deutsch, C., S. Emerson, and L. Thompson (2006), Physical-biological interactions in north pacific oxygen variability, *J. Geophys. Res.*, *111*, C09S9, doi:10.1029/2005JC003179.

Doney, S. C., V. J. Fabry, R. A. Feely, and J. A. Kleypas (2009), Ocean acidification: The other CO_2 problem, *Annu. Rev. Mater. Sci.*, *1*, 169–192, doi:10.1146/annurev.marine.010908.163834.

Dore, J. E., R. Lukas, D. W. Sadler, M. J. Church, and D. M. Karl (2009), Physical and biogeochemical modulation of ocean acidification in the central North Pacific, *PNAS*, *106*, 12,235–12,240.

Dunne, J. P., et al. (2012), GFDL's ESM2 global coupled climate-carbon Earth System Models Part I: Physical formulation and baseline simulation characteristics, *J. Climate*, *25*, 6646–6665, doi:10.1175/JCLI-D-11-00560.1.

Friedrich, T., et al. (2012), Detecting regional anthropogenic trends in ocean acidification against natural variability, *Nature Clim. Change*, *2*, 167–171.

Gent, P. R., et al. (2011), The community climate system model version 4, *J. Climate*, *24*, 4973–4991.

González-Dávila, M., J. M. Santana-Casiano, M. J. Rueda, and O. Llinás (2010), The water column distribution of carbonate system variables at the ESTOC site from 1995 to 2004, *Biogeosciences*, *7*, 3067–3081.

Hanawa, K., and L. D. Talley (2001), Mode waters, in *Ocean Circulation and Climate*, edited by G. Siedler, and J. Church, International Geophysics Series, pp. 373–386, Academic Press, New York, NY.

Hofmann, G. E., J. P. Barry, P. J. Edmunds, R. D. Gates, D. A. Hutchins, T. Klinger, and M. A. Sewell (2010), The effects of ocean acidification on calcifying organisms in marine ecosystems: An organism to ecosystem perspective, *Annu. Rev. Ecol. Evol. S.*, *41*, 127–147.

Molines, J.-M., B. Barnier, L. Penduff, T. Brodeau, A.-M. Treguier, S. Theetten, and G. Madec (2010), CO2calc–A user-friendly seawater carbon calculator for Windows, Max OS X, and iOS (iPhone).

Orr, J. C., et al. (2005), Anthropogenic ocean acidification over the twenty-first century and its impact on calcifying organisms, *Nature*, *437*, doi:10.1038/nature04095.

Orr, J. C. (2011), Recent and future changes in ocean carbonate chemistry, in *Ocean Acidification*, edited by J. P. Gatuso, and L. Hansson, pp. 41–66, Oxford University Press, Oxford.

Pörtner, H. O. (2008), Ecosystem effects of ocean acidification in times of ocean warming: A physiologists view, *Mar. Ecol. Prog. Ser.*, *373*, 203–217.

Raven, J., et al. (2005), *Ocean Acidification due to Increasing Atmospheric Carbon Dioxide*, 68 pp., Royal Society, London, UK.

Rodgers, B., K. B. Blanke, G. Madec, O. Aumont, P. Ciais, and J.-C. Dutay (2003), Extratropical sources of Equatorial Pacific upwelling in an OGCM, *Geophys. Res. Lett.*, *30*, 1084, doi:10.1029/2002GLO16003.

Sabine, C. L., et al. (2004), The oceanic sink for anthropogenic CO_2, *Science*, *305*, 367–371, doi:10.1126/science.1097403.

Séférian, R., D. Iudicone, L. Bopp, T. Roy, and G. Madec (2012), Water mass analysis of effect of climate change on Air-Sea CO_2 Fluxes: The Southern Ocean, *J. Climate*, *25*, 3894–3908, doi:http://dx.doi.org/10.1175/JCLI-D-11-00291.1.

Taylor, K. E., R. J. Stouffer, and G. A. Meehl (2012), An overview of CMIP5 and the experiment design, *Bull. Amer. Meteor. Soc.*, *99*, 485–498, doi:10.1175/BAMS-D-11-00094.1.